International Journal Of
Industrial Electronics Control and Optimization
Print ISSN: 3517-2645
Online ISSN: 3568-2645
Homepage: https://ieco.usb.ac.ir/

Expanding Generator Flexibility Regions in Renewable-Rich Grid via Optimal Transmission Switching and Dynamic Line Rating

Ali Beiranvand [1] | MahmoudReza Shakarami [2] | Meysam Doostizadeh [3]

Faculty of Engineering, University of Lorestan, Khorram Abad, Iran.[1,2,3]
Corresponding author's email: Doostizadeh.m@lu.ac.ir

Article Info

Article type:
Research Article

Article history:
Received: 25-November-2025
Received in revised form:
07-February-2026
Accepted: 13-February-2026
Published online: **********

Keywords:
Dynamic line rating,
Flexibility region,
Optimal transmission switching,
Renewable power generation,
Radar Scanning algorithm.

ABSTRACT

Today, power system operators face two major challenges: (1) determining the flexibility region for generators due to the increasing penetration of renewable generation in power systems, and (2) the rise in ambient temperature. Structural limitations in a power network and changes in its topology significantly affect the generator's flexibility region. In this paper, in addition to describing the structure of the flexibility region, the variability of these regions due to changes in the network topology is thoroughly demonstrated. For this purpose, the problem of determining the flexibility region of the generators (GFR) is integrated with the Optimal Transmission Switching (OTS) and Dynamic Line Rating (DLR) problems to develop the flexibility region and maximize the use of renewable power generation. To reduce the computational time and increase the effectiveness of the proposed method, an innovative method (referred to as Radar Scanning) is used to categorize the data related to the changes in the output power of renewable generation units. To evaluate the proposed method, the IEEE 30-bus and 118-bus power systems are employed, and the numerical results obtained from the simulation show that: first, OTS and DLR can enhance and improve the flexibility region of the generators in a power system; and second, by employing the proposed algorithm, the flexibility region of 30- and 118-bus power systems are determined by examining only a limited number of data (less than 30%), resulting in a 92% and 89% reduction in computational time, respectively.

NOMENCLATURE

DLR, DTR	Dynamic Line/ Thermal Rating	M , Ms	positive number related to the Big M method
DNE	DO-Not-Exceed limit	P_i	Base case output power of conventional unit *i*
DR	Dispatchable Region	P_{Dj}	Demand load on bus *j*
GFR	Generator Flexibility Region	R_i^+, R_i^-	Ramp-up/down limit of conventional unit *i*
LP	Linear Program	$\omega_k^e, \Delta\omega_k$	Forecasted and Uncertain output of renewable power generation unit *k*
MILP	Mixed-Integer linear program	π_{kl}	Power Transfer Distribution Factors (PTDF)
ODPs	Observed Data Points	P_i^{min}, P_i^{man}	The min/max generation of conventional unit *i*
OPF	Optimal Power Flow	H, h	matrix corresponding to the GFR
OTS	Optimal Transmission Switching	N_{sw}	Maximum number of lines for switching
PABs	Potentially Active Boundaries	θ_{max}	Maximum value of voltage angle in each bus
SOPs	soft open points method	P_i^+, P_i^-	A positive/negative change in the output of the conventional unit *i*
STR	Static Thermal Rating	y	value corresponding to P_i^+ and P_i^-
A, B, C, b0	Coefficient matrix of power system	Z_l	Binary variable for line state (1=closed,0=open)

F_l,B_l	Capacity/Susceptance of transmission line L	S^+, S^-	Slack variables

I. Introduction

With the beginning of the 21st century, due to the challenges caused by air pollution and the increasing cost of fossil fuels, the use of renewable resources such as wind and solar power has been increasing [1], [2], [3]. The increased use of renewable energy, due to its variability and high uncertainty (particularly wind power) along with rising ambient temperature, creates challenges for power systems and affects their flexibility, security and reliability.

To carry out preventive and corrective measures in the presence of renewable power generation units and to adapt the power system to them, many studies have been conducted in recent years. To operate power systems reliably and economically with renewable power generation, proposed methods often focus on adapting the power system by limiting the amount of renewable power generation. One such method is the "Do-Not-Exceed" concept, which defines the maximum range of renewable power generation that the power system can accommodate while maintaining security and reliability with minimal operational challenge [4]. The concept of the admissible region for renewable power generation is another method used in [5], [6] to assess power system risk. Another related concept is the Dispatchable Region (DR) of renewable power generation, which refers to the amount of power that the power system can tolerate. In other words, the DR represents the wind or solar power output that the power system can adapt to under given operating conditions [7], [8]. According to the research presented in [9], instead of examining all possible dispatchable regions, only the output data from renewable power generation units needs to be evaluated. This approach significantly reduces the number of boundaries that must be defined for the dispatchable region, as some theoretical boundaries will never be activated by actual renewable power outputs, making their determination unnecessary. Therefore, the concept of potentially active boundaries (PABs) was introduced.

In the research conducted in over recent years, most authors have focused on determining the flexibility and security regions of the power system in the presence of renewable sources. For example, [10] investigated problems in active distribution networks caused by the increased penetration of distributed generators (DGs) and proposed solutions to enhance network flexibility using control measures. Reference [11] explored improving flexibility and, consequently, the reliability and economy of power networks using the Soft Open Points (SOPs) method. Reference [12] examined the effect of transmission line switching on the flexibility of networks with wind power generation and showed that transmission switching can increase the network's flexibility with respect to renewable sources. Reference [13] described the security region of the power system in response to increasing renewable resource injection.

The flexibility region of generators is limited by network equipment, such as the thermal capacity of transmission lines and the reserve capacity of conventional generators. The injection of power from renewable energy sources into the power system buses can lead to overloading in the lines connected to those buses or elsewhere in network.

According to past studies, power transmission limitations in power system lines can be improved through two methods: optimal transmission switching (OTS) and the dynamic line rating determination system (DLR), also known as dynamic thermal rating (DTR) [14], [15]. The concept of OTS was introduced by [16]. This approach combines the OTS problem with the optimal power flow (OPF) problem, enabling to the relief or reduction of power system congestion and overload while maintaining network reliability at a desirable level. Past works have utilized OTS for various purposes, including achieving economic benefits, reducing operating costs, relieving line congestion, mitigating overload, serving as a corrective mechanism for voltage violations, and improving power system reliability [17].

Typically, most studies related to load flow or economic dispatch use the static thermal rating (STR), a specified and fixed value determined by assuming the worst-case weather conditions along a transmission line route [18]. However, as noted in [19], [20], if the atmospheric and environmental conditions around each line or conductor are known, the instantaneous and subsequently the dynamic thermal capacity can be determined. Studies indicate that implementing DLR can increase transmission line capacity by 15-50% in many cases and up to 150% of its STR capacity in others [21]. Furthermore, utilizing DLR capacity can reduce network congestion [22], enhance power system reliability [23], and consequently, defer or prevent the construction of new lines [24]. Reference [25] simultaneously examines the impact of using the dynamic capacity of lines and transformers to increase renewable generation injection, showing that using transformer dynamic capacity requires greater care due to its impact on reducing their useful life. Reference [26] comprehensively examines power grid transmission capacity optimization using DLR, demonstrating that this solution can mitigate the challenges associated with increased renewable resource usage .

A review of the literature reveals that prior research has predominantly focused on the mathematical determination and definition of power system flexibility or dispatchable regions. However, the impact of structural changes within

the power system on these generator flexibility regions has been largely unexplored. Structural changes in a power system can include line exits, changes in the number of generation units, changes in the thermal capacity of lines, and similar factors, which can cause changes in the size of the flexibility region.

Furthermore, existing methodologies lack an efficient algorithm for processing and classifying the output data from renewable sources. This shortcoming increases computational complexity and computational time, rendering previous approaches less practical for large-scale network analysis.

Motivated by the global imperative to integrate renewable resources and address challenges such as rising ambient temperature, this paper investigates a data-driven approach for determining flexibility regions. Specifically, it examines how these regions are affected by network topology changes via OTS and capacity adjustments via DLR. A key contribution of this work is the introduction of an algorithm to identify the most impactful line for DLR deployment—a step that not been addressed in earlier works—to maximize the expansion of the system's flexibility region.

In this paper, a new formulation using a data-driven method formulated as a linear programming (LP) problem with high computational efficiency for determining the generator flexibility region is introduced. Its main innovations are as follows:

1- It reduces the complexity of determining the flexibility regions of power systems using a newly proposed model, transforming the problem from a MILP to an LP problem, and increases its efficiency for analyzing large-scale systems.

2- A heuristic algorithm called “Radar Scanning” is introduced to classify and cluster the output data of renewable resources thereby increasing computational speed and reducing computation time.

3- A heuristic algorithm is introduced to identify the most effective transmission line for installing the DLR system in order to achieve the greatest impact on the network flexibility region.

II. Defining the Dispatch Problem and GFR

A) Mathematical Formulation Related to Load Flow in a Power System

Inspired by [9], the generator flexibility region (GFR) of a power system is defined as the set of all possible renewable power generation outputs under which the system can maintain secure and reliable operation within acceptable limits. The boundaries of the GFR are constrained by the physical limits of network equipment. Therefore, the aim of this section is to determine the maximum possible GFR subject to these operational conditions. If the power output of conventional units is denoted by P_i and the power output of renewable generation is denoted by ω^e, the equations describing variations in generation and transmission power are formulated as follows.

$$\sum_i (P_i + P_i^+ - P_i^-) + \sum_k (\omega_k^e + \Delta\omega_k) = \sum_j P_{Dj} \quad (1)$$

$$-F_l \le \sum_i \pi_{il}(P_i + P_i^+ - P_i^-) + \sum_k \pi_{kl}(\omega_k^e + \Delta\omega_k) - \sum_j \pi_{jl} P_{Dj} \le F_l, \ \forall l \quad (2)$$

$$P_i^{min} \le P_i + P_i^+ - P_i^- \le P_i^{max}, \quad \forall i \quad (3)$$

$$0 \le P_i^+ - \le R_i^+, \quad \forall i \quad (4)$$

$$0 \le P_i^- - \le R_i^-, \quad \forall i \quad (5)$$

Where, equation (*1*) represents the power balance. Inequality (*2*) enforces the security limits on the maximum transmission power of the lines, which must remain within the range (F_l and -F_l) under all conditions. Constraint (*3*) is the maximum and minimum power generation capacity of the conventional units. Constraints (*4*) and (*5*) govern the upward and downward reserve capacity of each conventional unit. Due to changes in renewable energy generation, it is necessary to adjust the output of conventional units according to the corresponding reserve capacity. In equations (*1*) to (*5*), the variables P^- and P^+ represent changes in the power output of conventional generation units following a change $\Delta\omega$ in renewable power generation.

B) Formulation of the Generator Flexibility Region

In general, all equality and inequality constraints from (*1*) - (*5*) can be compactly expressed in the following form.

$$AP + B\begin{bmatrix} P^+ \\ P^- \end{bmatrix} + C(\omega^e + \Delta\omega) \le b_0 \quad (6)$$

Where, the coefficients from the power system constraints (*1*) - (*5*) are represented by matrices A, B, C, and the vector b_0. In equation (*6*), the variable $\begin{bmatrix} P^+ \\ P^- \end{bmatrix}$ can be substituted with a new variable y. Furthermore, since ω^e is a constant, the corresponding terms in inequality (*6*) can be moved to the right-hand side. Thus, the formulation can be rewritten as follows:

$$AP + By + C\Delta\omega \le b \quad (7)$$

Where, $b = b_0 - C\omega^e$.

Finally, the generator flexibility region can be defined as follows [27]:

$$W^{GFR} = \{\Delta\omega | \exists y: By + C\Delta\omega \le b - AP\} \quad (8)$$

The region W^{GFR} defined in equation (*8*) is formed by the boundary lines or planes arising from the power system constraints given in equations (*1*) - (*5*). Research in [9] indicated that ODPs activate only a limited subset of these GFR boundaries, termed Potentially Active Boundaries (PABs). A boundary of the GFR is activated mathematically whenever a set of ODPs violates inequality (*8*). It was demonstrated in [27] that inequality (*8*) can be reformulated as follows.

$$W^{GFR} = \begin{Bmatrix} \Delta\omega | u^T(C\Delta\omega) \ge u^T(b - AP), \\ \forall u \in vert(U) \end{Bmatrix} \quad (9)$$

$$U = \{u | B^T.u = 0, \quad -1 \le u \le 0\} \tag{10}$$

Where $vert\ (U)$ denotes the set of vertices of polyhedron U, and the superscript T represents the matrix transpose. The activation condition for a boundary I of the GFR is:

$$I = \{\exists \Delta\omega \in \Omega, u^T(C\Delta\omega - b + AP) < 0\} \tag{11}$$

Where Ω denotes the total observed points related to the outputs of renewable power generation.

C) Process for Determining the GFR Boundaries

The process for determining the boundaries of the GFR follows a methodology similar to the one described in reference [9] for determining the dispatchable region. The key distinction, however, is that this paper formulates the final problem as a Linear Programming (LP) model, whereas the reference method uses a Mixed-Integer Linear Programming (MILP) problem. A further significant contribution of the proposed method is its use of an innovative data categorization and ranking technique to identify and evaluate the effective data points critical for defining the GFR boundaries. This technique will be detailed in the subsequent section. The objective is to determine the active boundaries, provided that the union of the regions outside the GFR, resulting from both the current boundary and all previously identified boundaries, is either an empty set or remains mutually exclusive with any existing region. Mathematically, the activation condition for a boundary is equivalent to:

$$W_1' \bigcup \emptyset = \boldsymbol{D} \rightarrow \begin{cases} if\ \boldsymbol{D} = \emptyset \rightarrow PAB_1\ is\ deactive. \\ if\ \boldsymbol{D} \neq \emptyset \rightarrow PAB_1\ is\ active. \end{cases}$$

$$W_i' \cap \left(\bigcup_{j=1}^{i} W_j' \right) = \boldsymbol{k} \tag{12}$$

$$\begin{cases} \boldsymbol{k} = \emptyset \rightarrow PAB_i\ is\ active. \\ \boldsymbol{k} = W_j' \rightarrow PAB_j\ is\ deactive\ \&\ PAB_i\ is\ active. \\ \boldsymbol{k} = W_i' \rightarrow PAB_i\ is\ deactive. \\ \boldsymbol{k} = W^{"}, W^{"} \neq W_i', W^{"} \neq W_j' \rightarrow PAB_i\ is\ active \end{cases}$$

Where W_i' and W_j' represent the regions outside the GFR, separated by boundaries i and j, respectively.

The logic of Equations (12) follows that after evaluating each point of the ODPs set using the proposed algorithm, the conditions related to set **D** (the first two equations in (12)) are checked first. This step aims to activate effective boundaries while preventing the activation of ineffective or redundant ones.

The procedure is as follows:

a) For boundary number 1, the condition is compared with the empty set ϕ. If W_1' has no members (i.e. **D**=ϕ), no boundary is activated. If it has members (i.e. **D**≠ ϕ), then boundary PAB_1 is activated.

b) For any subsequent boundary *i* activated by the ODPs, the second part of Equation (12) (involving set **k**) must be examined. The set of points separated by the new boundary *i* (W_i') is compared with the union of all points outside the final flexible from previously active boundaries:

Criterion 1: If W_i' adds new points to the total excluded set, boundary *i* is accepted as a new boundary, otherwise no new boundary is created.

Criterion 2: If all points excluded by a prior boundary *j* are entirely contained within W_i' (i.e., $W_i' \cap \left(\bigcup_{j=1}^{i} W_j'\right) = W_j'$), then boundary *j* becomes ineffective and is removed and replaced by boundary *i*.

The conditions specified in (12) are used to prevent the formation or activation of ineffective boundaries for the GFR. The proposed process for determining the W^{GFR} space in this paper is as follows:

Step 1) The initial operating point values of the system (P_i and ω_k^e) are determined.

Step 2) All ODPs are represented as Ω set.

Step 3) The phase and magnitude values of all ODPs are determined in polar coordinates and sorted based on their phase value.

Step 4) The data space is divided into N_{scan} segments, and all data points are allocated to these segments based on their phase values. Within each segment, the data points are sorted in descending order of magnitude.

Step 5) The counter for the parts inside the space is set to SC_n=1.

Step 6) The highest-ranked (largest magnitude) data point within segment SC_n is assigned to $\Delta\omega_k$, represented by the counter k=1.

Step 7) The GFR (W^{GFR}) is initially assumed to be sufficiently large to contain all ODPs. This can be formulated as $W^{GFR} = \{\Delta\omega | H.\Delta\omega \ge h\}$, where matrix **H** and vector **h** are updated iteratively during the boundary determination process.

Step 8) If $\Delta\omega_k$ satisfies the condition in step 7, problem (13)-(15) is considered solved for it. In this case, the segment counter k is incremented by one. If the condition is not satisfied, the next data point with the largest magnitude will be selected from the same segment ($k = k + 1$). To determine the boundary of the GFR, the following LP problem is solved for the output data $\Delta\omega_k$.

$$\max u^T\ (b - AP - C\Delta\omega_k) \tag{13}$$

$$s.t.: B^T.u = 0 \tag{14}$$

$$-1 \le u \le 0 \tag{15}$$

Step 9) If the constraint $u^{*T}(C\Delta\omega_k) \ge u^{*T}(b - AP_i)$ is satisfied for the optimal solution u^*obtained from the problem (13)-(15), then there is no need to establish a new boundary, and the algorithm returns to step 8. However, if the constraint $u^{*T}(C\Delta\omega_k) \ge u^{*T}(b - AP_i)$ is not satisfied, the existing GFR (W^{GFR}) is updated by adding a new boundary as $W^{GFR} = W^{GFR} \cap \{u^{*T}(C\Delta\omega - b + AP) \ge 0\}$ and considering equations (13)-(15). The values of matrix **H** and vector **h** are updated by adding the values of $u^{*T}C$

and $u^{*T}(b - AP)$, respectively. The algorithm then proceeds to step 10.

Step 10) The condition presented in equation (12) is applied to select the active boundary and then returned to step 6.

Step 11) the value of counter k is incremented by one unit.

Step 12) If SC_n is less than the total number of segments, it adds one unit, and then the algorithm returns to step 6. Otherwise, the algorithm proceeds to step 13.

Step 13) End.

By executing the above algorithm, if any ODPs from the set Ω within a segment violate the condition $u^{*T}(C\Delta\omega_k - b + AP) \geq 0$, the corresponding boundary line will be activated.

III. Formulating the OTS in the Presence of Renewable Sources

The GFR in a power system is not rigid or fixed, as it depends heavily on the network structure. Changes in the network structure, such as taking transmission lines out of service, can cause variations in these regions. Therefore, this variable characteristic of the GFR can be utilized and developed according to the needs of the power system operators. One available corrective measure is OTS. The concept of OTS involves temporarily taking one or more transmission lines out of service at specific times to allow the power system to operate more efficiently. OTS can be implemented based on either AC Optimal Power Flow (ACOPF) or DC Optimal Power Flow (DCOPF). However, due to its simplicity, reasonable accuracy, and computational speed, DCOPF is typically preferred for research studies. Consequently, this paper employs DCOPF to assess the impact of OTS on the GFR. According to [28], [29], integrating OTS and DCOPF can be expressed as problem (16)-(23), which is a MILP problem.

$$\min \sum_i C_i P_i \tag{16}$$

$$-P_l + B_l(\theta_i - \theta_j) + M(1 - Z_l) \geq 0, \quad l \in L \tag{17}$$

$$-P_l + B_l(\theta_i - \theta_j) - M(1 - Z_l) \leq 0, \quad l \in L \tag{18}$$

$$\sum_{i \in g} P_i - \sum_{i \in D} P_{Di} = \sum_{l \in L} P_l \tag{19}$$

$$-\theta_{max} \leq \theta_i - \theta_j \leq \theta_{max} \tag{20}$$

$$P_i^{min} \leq P_i \leq P_i^{max} \tag{21}$$

$$-Z_l . F_l \leq P_l \leq Z_l . F_l \tag{22}$$

$$\sum_{l \in L} (1 - Z_l) \leq N_{sw} \tag{23}$$

Where, expression (16) denotes the objective function. Inequalities (17) and (18) define the power flow on each line and its relationship to the voltage angles at the terminal buses. In these constraints, the Big-M parameter is a sufficiently large positive constant and Z_l is a binary variable representing the on/off status of line l (where $Z_l = 1$ indicates the connected line and $Z_l = 0$ indicates a disconnected line). Equation (19) enforces the balance of generation, consumption and transmission power at each bus. Constraints (20) - (22) impose limits on bus voltage angle differences, the active power output of the conventional generators, and the line transmission capacities, respectively. Constraint (23) restricts the maximum number of permitted switching operations in the system.

To adapt the OTS problem formulated in (16)-(23) for purpose of improving the GFR, several specific modifications are required. Accordingly, The proposed OTS formulation for improving the GFR in this paper is as follows.

$$\min \sum_{i \in bus} [M_s . (S_i^+ + S_i^-)] \tag{24}$$

s.t: (17), (18), (20), (22), (23)

$$\sum_i (P_i + P_i^+ - P_i^-) + \sum_i (S_i^+ - S_i^-) + \sum_k (\omega_k^e + \Delta\omega_k) - \sum_j P_{Dj} = \sum_{l \in L_{bus}} P_l \tag{25}$$

$$\sum_i (P_i^+ - P_i^-) \leq \sum_k \Delta\omega_k \tag{26}$$

The objective function of the resulting MILP problem is given in equation (24). Its purpose is to minimize the costs associated with the increasing or decreasing the power output of conventional units. The variables S_i^+ and S_i^- are slack variables similar to P_i^+ and P_i^-, introduced to ensure the problem's feasibility. The coefficient M_S, a large positive number, penalizes these slack variables to minimize their values under normal power system conditions. These slack variables measure the deviation in output of conventional units from their allowable reserve capacity limits. Equation (25) represents the DC power balance constraint at each bus, which now includes the power from renewable generators as well as the adjustments from conventional units. Inequality (26) is a new condition introduced in this paper. It states that the total adjustments (increase or decrease) in conventional generation must be less than or equal to the total change in renewable power output.

It is important to note that a power system's operating state can change with variations in renewable generation output. Finding a single optimal switching solution for all possible operating points can be computationally prohibitive or infeasible. To address this and find an optimal solution for problem (24)-(26) given a specific change in renewable output $\Delta\omega_k$, the following procedure is adopted.

1-The data points already identified during the determination of W^{GFR} by solving problem (13)-(15) are not required to be re-evaluated in the OTS problem (24)-(26). Only points outside the current W^{GFR} require assessment. The rationale is that if a feasible OTS solution exists for a point outside W^{GFR}, the constraints (13)-(15) guarantee a

solution for all points inside it. Conversely, if no feasible solution exists for points outside W^{GFR}, the status of interior points becomes irrelevant for this specific $\Delta\omega_k$.

2- As stated above, since problem (24)-(26) is evaluated for all points outside W^{GFR}, the resulting binary variable Z_l (line status) are stored for every such ODP and for each step.

3- The sorted Z_l values are then analyzed to determine the optimal line(s) to switch out for the given $\Delta\omega_k$. The line or set of lines with the highest frequency of $Z_l = 0$ across the evaluated points is selected as the optimal switching action.

4- After identifying the line(s) to be taken out of service, the system matrices **A**, **B**, **C**, and vector **b** in (*1*)-(*5*) are updated according to the new network topology. The proposed algorithm from section II is then repeated for points outside the initial W^{GFR} to determine a new, enhanced flexibility region, denoted W^{GFR-S}.

It is possible that the GFR may decrease if a transmission line is taken out of service for non-optimal reasons (e.g., maintenance or outage due to a fault). Such an outage can change the power flow on the lines, potentially causing congestion on other lines and reducing the system's ability to adapt to changes in renewable power generation. Consequently, system operators must re-evaluate the GFR following any change in network topology.

IV. Effect of DLR on the GFR

Transmission lines are affected by various atmospheric conditions and environmental factors, including ambient temperature, wind speed, altitude, time of day, and angle between wind and conductor. These factors cause the thermal capacity of transmission lines to be time-varying. In power system studies, a fixed Static Thermal Rating (STR) is often used to limit the line power flow. This rating (capacity) is determined based on the worst-case conditions for the line, which can be a conservative estimate for many hours of the day or even for most times of the year. In recent years, significant research has focused on using DLR systems [17]. Various systems are now employed to determine the real-time dynamic capacity of power lines, enabling the control of current flow at any given moment [30]. Conductor temperature depends on the current passing through it. If the current exceeds the permissible limit, the conductor temperature rises. This can reduce the required clearance to the objects below and, in more severe cases, cause the conductor temperature to exceed safe limits, reducing mechanical strength and potentially leading to line damage. The detailed calculations describing how line thermal capacity varies with environmental conditions are fully explained in references [19], [20]. This paper utilizes the results from a hypothetical DLR system installation for analytical purposes.

To assess the effect of the DLR system on the GFR, the first step is to identify the transmission line that limits the GFR. For this purpose, the power flow through the lines is calculated using constraint (*2*) for the data points inside the GFR that are closest to its active boundary. The line(s) with power flow values near their static thermal capacity are then identified as the limiting line(s). Consequently, the GFR can be expanded or contracted by adjusting the power transmission capacity of these line(s).

The algorithm for evaluating the effect of changing line thermal capacity on the GFR is as follows.

Step 1) the limiting line is identified as described above.

Step 2) the thermal capacity of the limiting line is adjusted by a percentage of its static thermal rating. This adjustment can be an increase or decrease.

Step 3) Using Equations (*1*)-(*5*), the coefficients **A**, **B**, **C** and **b** are updated.

Step 4) the algorithm proposed in Section II is repeated for all points outside the initial W^{GFR} to determine a new region, denoted W^{GFR-L}.

V. Introducing the Innovative Algorithm for Classifying Renewable Power Output Data

Reducing computation time in large-scale power systems is primary concern. For this purpose, an innovative classification method called the "Radar Scanning" algorithm is introduced to categorize the output data of renewable units, thereby decreasing the overall calculation time.

A) Data Classification Based on Innovative Radar Scanning Algorithm

If the number of buses with renewable power generation is n_w, the analytical space of the flexibility region is n_w-dimensional. Analyzing and understanding an n_w-dimensional space, where n_w>3, is extremely complex. To simplify the analysis of renewable generation output points, a two-dimensional space is utilized. The output data from n_w different network buses are examined pairwise within a two-dimensional space to determine their positions. The two-dimensional Radar Scanning algorithm is then applied to classify the data. In an n_w-dimensional space, the number of possible two-dimensional subspaces created is given by:

$$n_{2D} = \frac{n_w!}{(n_w - 2)!\,2!} \tag{27}$$

Where n_{2D} represents the total number of n_{2D} subspaces established in an n_w-dimensional space. For all data points corresponding to the changes in renewable power output ($\Delta\omega_k$), their phase and magnitude values in polar coordinates are determined as follows.

$$\begin{aligned} &\Delta\omega_k = r_k \angle\theta_k \ , \qquad 0 \le \theta \le 2\pi \\ &r_{ki} = \sqrt{\Delta\omega_{ki,1}^2 + \Delta\omega_{ki,2}^2} \\ &\theta_{ki} = \tan^{-1}\left(\Delta\omega_{ki,2}^2 / \Delta\omega_{ki,1}^2\right) \end{aligned} \tag{28}$$

Where r is the magnitude and θ represents the phase of the data in the two-dimensional subspace i. The polar representation of a renewable generation output point is illustrated in **Fig. 1**. To enhance the algorithm's effectiveness, it is preferable to use the magnitude of the data point in the original n_w-dimensional space for the value of r in Equation (28). In general, increasing the number of segments improves the accuracy of the program at the cost of longer calculation time. The number of segments can be selected between 20 and 72, resulting in a segment angle ranging from 18° to 5°.

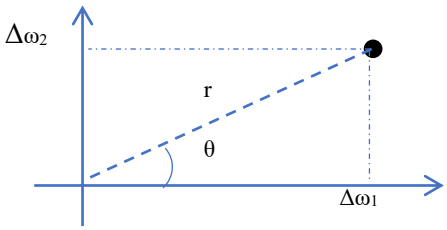

Fig. 1. Polar coordinate representation of a ODP.

The data space division by the Radar Scanning method is shown in **Fig. 2**. The scanning process and division of the region proceeds counterclockwise, starting from the positive horizontal axis. To facilitate a clearer understanding of the proposed innovative Radar Scanning algorithm in two-dimensional space, the steps for its application are presented sequentially as follows.

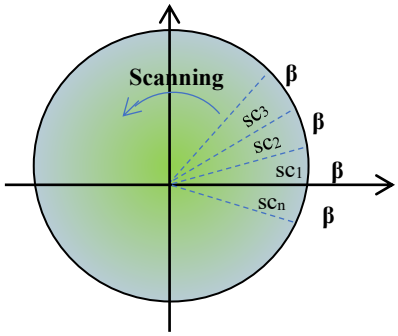

Fig. 2. Data space segmentation via the Radar Scanning algorithm.

Radar Scanning Algorithm

1- For each data point, the dominant two-dimensional subspace is determined by identifying its two components with the largest magnitudes.

2- Within each identified two-dimensional subspace i, the amplitude and phase of all points are calculated using Equation (28)*. It is recommended to use the point's magnitude the original n_w-dimensional space rather than its magnitude in the two-dimensional subspace.*

3- All points in the subspace are sorted in ascending order based on their phase value.

*4- The two-dimensional subspace i is divided into SC_n equal angular segments (see **Fig. 2**), and points are assigned to segments according to their phase.*

5- Within each segment, the points are sorted again, this time in descending order based on their overall n_w-dimensional magnitude.

B) Process of the Innovative Radar Scanning Algorithm

Analytically, the GFR is continuous and lacks singular points. Consequently, it is not necessary to evaluate all renewable output data points. Instead, only the highest-ranked points by magnitude within each segment need to be assessed. For this purpose, the process begins with the first segment (lowest phase angle), selecting the top-ranked point (largest magnitude). If this point satisfies the condition in **step 7** of the algorithm from section II-C (i.e., lies within the current GFR), the algorithm processes only this point and moves to the next segment. If the selected point does not satisfy the condition (i.e., lies outside the GFR), it is recorded as an external point, and the next highest-ranked point within the same segment is evaluated. This process repeats for all segments. The algorithm' counter-clockwise traversal of the two-dimensional subspace resembles the operation of a military radar system, hence the name "Radar Scanning".

This method ensures that all points near the GFR boundary are evaluated while avoiding unnecessary computation on low-ranking interior points that do not define the region's limits. This significantly reduces the overall computational time.

VI. Numerical Simulation Results

This section, analyzes the proposed methods and algorithms for the developing and modifying the GFR through OTS and DLR. The simulation results are compared against a base case that applies neither corrective action. All simulations are performed on the IEEE 30-bus and IEEE 118-bus test systems, with data from [31] and [9]. The parameter M is set to 20,000, and the reserve capacity of conventional units is set to 25% of their maximum output, following [27]. Simulations were executed on a PC with an Intel Dual Core E 5200 processor and 2.0 GB RAM.

1) Case 1: IEEE 30-Bus System Test

The IEEE 30-bus system comprises 30 buses and 41 transmission lines, with a total load of 189.2 MW and a maximum conventional generation capacity of 335 MW. To study the GFR in this test system, as per [9], renewable generation units with base generation capacities of 10 MW and 20 MW are installed at buses #1 and #22, respectively, resulting in a renewable penetration rate of 15.86%. The line loading under these base conditions is shown in **Fig. 3**. Lines 11, 28 and 32 exhibit the highest loading percentage and are most prone to congestion if the renewable power injection increases.

A dataset of 500 ODPs is used for renewable output (data-driven method). For this purpose, first, the GFR is determined for the base case without OTS or DLR.

A) GFR Determination without OTS and DLR

As outlined in section II, the GFR is determined by using the proposed method and innovative Radar Scanning algorithm applied to the ODP set. This is formulated as a LP problem ((13)-(15)), solved using the ODP data to establish a data-driven GFR. The base case GFR (i.e., without OTS and DLR) is shown in **Fig. 6**. The region is enclosed by a single active boundary. In this case, 72 ODPs lie outside the GFR (shown in red). The activated boundary is given by $[0 \quad -0.4864].\Delta\omega \geq [-0.1455]$. This boundary is primarily activated by increased power injection from the renewable generator at bus #22. The π coefficients for this bus and all transmission lines are shown in **Fig. 4**. Lines 1, 2, 6, 12, 16, 20, 32 and 33 have notably higher coefficients. As shown in**Fig. 5**, a gradual increase in power injection at bus #22 causes line #32 (between buses 21-22) to congest first, limiting further power transfer. This activated boundary must be considered as a constraint in power flow solutions to ensure secure system operation when renewable generation changes.

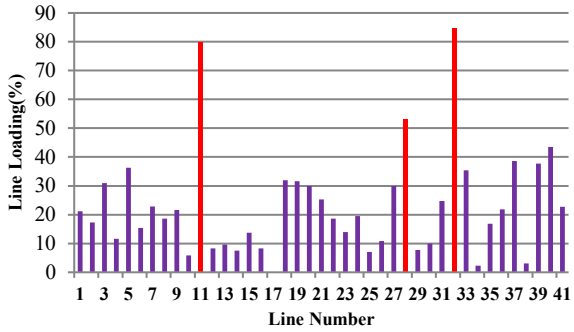

Fig. 3. Line loading percentages under base case condition.

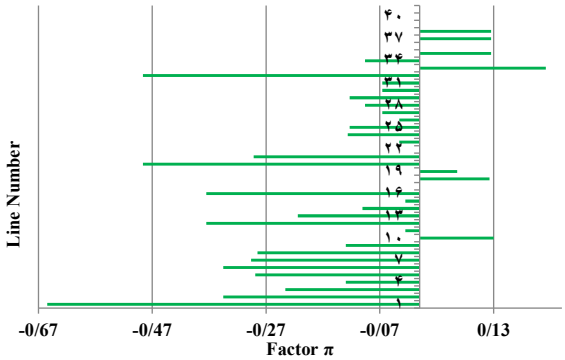

Fig. 4. π coefficients for power injection at bus 22.

It is important to note that the identification of the limiting line depends on several interconnected factors: the π coefficient, the initial line loading, and the line's capacity. This combination explains why line #32 becomes congested earlier than others. Specifically, an initial load exceeding 80%, a π coefficient of approximately 0.48, and a capacity of only 32 MVA, makes line #32 the most vulnerable to congestion. In contrast, although line #1 has the highest π coefficient (0.65), it does not congest due to its low initial loading (20%) and its significantly higher capacity (130 MVA).

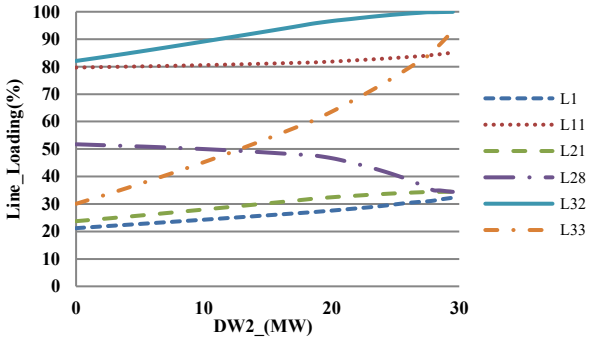

Fig. 5. Line loading progression with increased power injection at bus 22 (base case).

b) Effect of OTS on the GFR

This section analyzes the effect of OTS on the GFR using the algorithm proposed in Section III. The MILP problem formulation in (24)-(26) is applied to ODP points located outside the base GFR to identify the optimal transmission line that should be taken out of service.

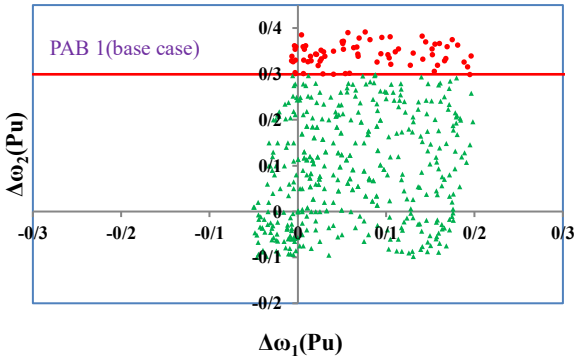

Fig. 6. Baseline GFR without corrective actions (base case).

In this system test, for the ODPs outside the GFR, line 20 (10-21) is identified as the optimal line to switch out, as it has the highest frequency of selection among all lines. **TABLE I** shows the selection count for each line, line 20 (10-21) has the highest value. For this analysis, the maximum number of allowed switching operations, N_{sw}, was set to 1. When N_{sw} is increased to 2, the optimal pair of lines to switch out are lines 20 (10-21) and 1 (1-2), in that order, as shown in the second column of **TABLE I**.

TABLE I Optimal Line Switching Frequencies for GFR Enhancement via OTS.

N_{sw}=1	N_{sw}=2
Line(No. of Selection)	Line(No. of Selection)
10-21(247)	10-21(190)
6-9(69)	1-2(175)
1-3(38)	22-24(53)
6-10(24)	23-24(40)
10-17(15)	6-8(38)

Following the switching of the selected line (20 (10-21)) and the subsequent update of the system matrices **A**, **B**, **C** and vector **b**, the GFR is recalculated using the proposed algorithm from Section II. The resulting region is shown in **Fig. 7**. A significant expansion of the GFR is observed after the switching action, incorporating many more ODPs. Consequently, the number of points outside the new GFR is reduced to only 9, compared to 72 in the base case. This development of the GFR through optimal switching enables the power system to accommodate a greater amount of power injection from renewable units without violating security constraints. The change in loading pattern of lines is shown in **Fig. 8**. As the figure indicates, line # 33 (22-24) becomes the new limiting constraint, congesting earlier than others. This outcome was predictable: switching out line 20 (10-21) fixed the power flow on the now-radial line 32 (21-22). Therefore, as renewable injection at bus #22 increases, the subsequent power flow — following the path indicated in **Fig. 5**— causes line 33 (22-24) to reach its thermal limit first.

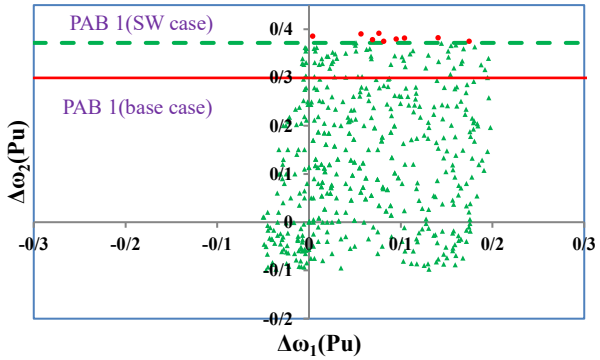

Fig. 7. Expansion of the GFR with OTS.

c) Effect of DLR on GFR

This section evaluates the impact of the Dynamic Line Rating (DLR) system on the GFR, assuming the DLR system has been optimally installed on a transmission line that limits power transfer. While the optimal placement methodology of the DLR system itself is beyond the scope of this paper, guidelines are provided in section IV. For this analysis, a DLR system is assumed to be installed on a suitable line. Its output is modeled as a percentage of the line nominal static thermal rating and incorporated into the algorithm from section IV. For the test system, the proposed algorithm identifies line 32 (21-22) as the most suitable candidate for DLR installation. To analyze the sensitivity, the line's dynamic capacity is set to 0.95 and 1.05 times its nominal static capacity, reflecting the environmental and atmospheric conditions. After updating the coefficients **A**, **B**, **C** and **b** with these adjusted capacities, the resulting GFR regions are shown in **Fig. 9** and **Fig. 10**, respectively. The results clearly demonstrate that a reduction in transmission capacity of line 32 (21-22) contracts the GFR, whereas an increase in its capacity expands the region. Therefore, it can be concluded that at the time of connecting renewable power generations to the power system, it is necessary to carry out studies related to the thermal capacity of the lines at various times carefully so that the line does not get overloaded due to the injection of additional power in one bus of the network.

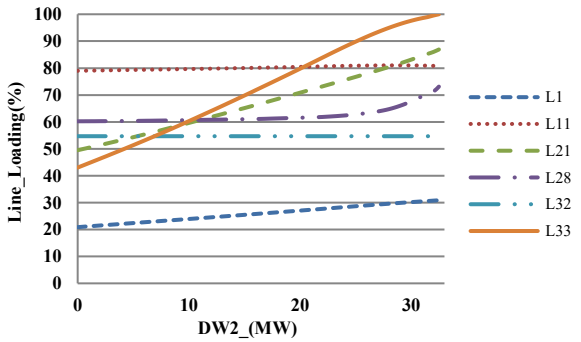

Fig. 8. Post-switching line loading analysis for increased power injection at bus 22.

Considering the arrangement of ODPs shown in **Fig. 6**, if Δω increases excessively, according to Equation (*1*), a reduction in the generated power of conventional generators is necessary to maintain power balance. If this required adjustment exceeds the reserve capacity of conventional generators defined by Equations (*3*) to (*5*), then Equation (*6*) and its dual condition, $u^T(b - AP - C\Delta\omega) \leq 0$, are violated. In addition, based on Equation (*2*), which is related to the thermal capacity of the lines, a high value of Δω, considering the π coefficients (shown in **Fig. 4**) and line flow dependencies, can increase the power flow in one or more lines beyond their nominal capacity. Consequently, Equations (*2*) and (*6*), along with the condition $u^T(b - AP - C\Delta\omega) \leq 0$, are violated.

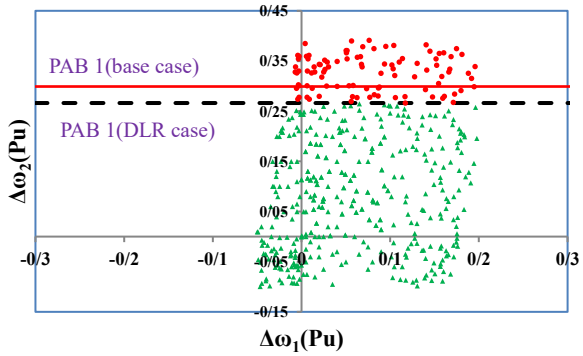

Fig. 9. GFR reduction under decreased line capacity with DLR.

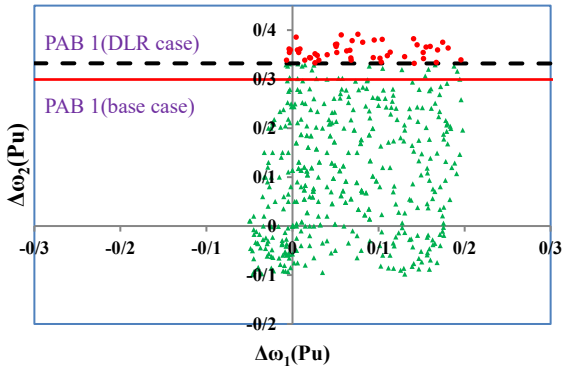

Fig. 10. GFR sensitivity to reduced line thermal limit.

Based on Inequality (*2*), it is possible to determine the capacity of the line 32 (21-22) in such a way that the active boundary that causes the most significant restriction for the GFR becomes inactive. As shown in **Fig. 9** and **Fig. 10**, boundary 1 (when active) excludes 98 and 48 ODPs from the GFR under different capacity conditions. Applying Inequality (*2*) to the outermost excluded point yields an optimal capacity of 37.3 MVA for line 32 (21-22), which is 16.6% above its nominal static capacity. Applying this change in the problem deactivates the boundary 1, incorporates all ODP points into the GFR, and thereby expands the region. **Fig. 11** shows the resulting GFR and confirms that the capacity adjustment on line 32 (21-22) has inactivated the boundary and developed the GFR.

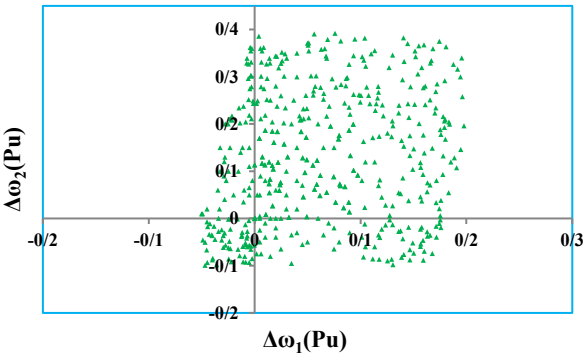

Fig. 11. GFR expansion via DLR enhancement (line 32(21-22)).

2) Case 2: IEEE 118-Bus System Test

To evaluate the proposed algorithm's scalability, it is analyzed on the IEEE-118 bus system described in reference [9] using 500 ODPs.

The IEEE 118-bus system comprises 118 buses and 185 transmission lines, with a total load of 4242 MW and a maximum conventional generation capacity of 5859.2 MW. To study the GFR in this test system, renewable generation units with base capacities of 170MW and 120MW are installed at buses #49 and #72, respectively, resulting in a renewable penetration rate of 6.84%.

The simulation results of the effect of OTS and DLR capacity utilization are shown in **TABLE II**. The limiting lines in this sample power system are 119 (69-77), 112 (65-68), 50 (30-38), 123 (71-72) and 120 (70-71), with initial loading of 93.28%, 27.8%, 89.54%, 37.44% and 37.7%, respectively. Optimal switching takes line 112 (65-68) out of service and, according to **TABLE II**, increases the GFR by about 10% compared to the base case. In this sample power system, using the algorithm proposed in Section IV, lines 120 (70-71) and 123 (71-72) are selected as the optimal lines for installing the DLR system. According to **TABLE II**, if the output of the DLR system increases the capacity of the mentioned lines by 15%, then the GFR increases by about 11.24%, and vice versa, if the capacity of the mentioned lines decreases by about 15%, the GFR also decreases by about 9.24%.

TABLE II Simulation results for the IEEE 118-bus test system.

Case	Number of ODPs inside the GFR	Increase in GFR compared to the base case (%)
Base	249	0
OTS	273	9.64
DLR (+15%) (increase mode for Lines 120 and 123)	277	11.24
DLR (-15%) (decrease mode for Lines 120 and 123)	226	-9.24

To evaluate and compare the performance of the proposed algorithm, its results are benchmarked against existing methods in **TABLE III**. The table clearly demonstrates that the proposed algorithm is significantly faster than previous approaches in both small- and large-scale systems, making it particularly suitable for large-scale applications.

TABLE III Performance comparison of the proposed algorithm with prior algorithms.

System Test	Number of ODPs	Computational time (s)		
		Without using the algorithm	With using the proposed algorithm	The proposed-nPrl algorithm in [9]
IEEE-30	250	17.52	0.9425	1.6292
Bus	500	36.44	3.0921	8.3078
IEEE-118	250	44.628	6.7112	11.8062
Bus	500	96.183	10.5783	29.378

TABLE III demonstrates that the Radar Scanning heuristic algorithm significantly enhances computational efficiency. By classifying data based on phase and amplitude, it reduces the calculation time for determining the GFR by approximately 92% for the 30-bus system (from 36.44 to 3.09 seconds) and 89% for the 118-bus system (from 96.183 to 10.5783 seconds), compared to not using the algorithm. In addition, the calculation time for determining the GFR with the method proposed in this paper for both the 30-bus and 118-bus test systems is much less than the method proposed in reference [9]. In the case of using 500 ODPs, the algorithm proposed in this paper reduces the computation time in the 30-bus test system by about 63% compared to the computation time of the method proposed

in reference [9] (3.0921 seconds versus 8.3078 seconds). This is also true for the larger system, i.e. 118 buses, and the proposed algorithm reduces the computation time by about 64% compared to the proposed method in the reference (10.5783 seconds versus 29.378 seconds). These results, summarized in **TABLE III**, strongly indicate the superior performance of the proposed algorithm for determining power system flexibility regions and optimizing the utilization of installed renewable generation capacity, especially in large-scale applications.

It is important to note that the time required to perform the GFR calculation and the accuracy of the result depend partly on the number of segments in the Radar Scanning (SC_n). **Fig. 12** shows the computation time and solution accuracy, number of points outside the GFR), as a function of the segment angle (the inverse of the number of segments). As can be seen from **Fig. 12**, the relationship between accuracy and time is inversely proportional. The greater the number of segments in the Radar Scanning method (i.e., the smaller the segment angle), the greater the solution accuracy, but the computation time also increases, and vice versa. Therefore, it is necessary to select a suitable trade-off between accuracy and speed by finding the optimal value for the number of segments in the Radar Scanning algorithm, as shown in **Fig. 12**.

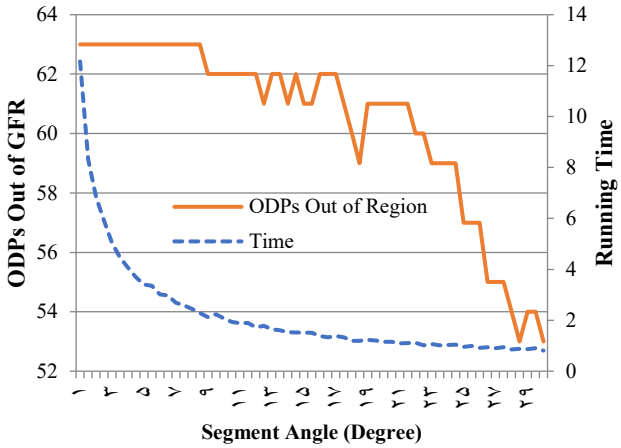

Fig. 12. Computational performance of the Radar Scanning algorithm for the 30-bus system

VII. Conclusion

This paper has focused on analyzing changes in the flexibility region of the generators (GFR) resulting from modifications to the network structure, specifically through optimal transmission line switching and thermal line capacity adjustments. The GFR was defined based on variations in renewable generation outputs, and two distinct methods were proposed to develop and expand this region: (1) Optimal Transmission Switching (OTS) and (2) utilization of Dynamic Line Rating (DLR). For each method, an iterative algorithm was introduced to efficiently solve associated MILP and LP problems. To reduce the computational time and enhance the effectiveness of the proposed method, an innovative Radar Scanning algorithm was introduced. This method classifies renewable generation output so that only the most critical points are evaluated, making the whole process much faster. The computational efficiency was further improved by restricting the OTS and DLR evaluations to data points lying outside the initial GFR region. The application of proposed algorithms demonstrated that OTS can expand the GFR, enabling greater permissible injection from renewable sources into the network. Similarly, by applying the DLR, which represents a percentage of its static capacity, the GFR also changes, so that with the increase of the limiting line thermal capacity, the GFR region expands, and with the decrease of this thermal capacity, the GFR contracts.

Several important aspects remain for future work. These include integrating the cost coefficients of conventional generation units to economically optimize the adjustments P^+ and P^-, as well as incorporating full AC power flow constraints into the proposed algorithms. Such measures allow for a more comprehensive and practical assessment of the solutions resulting from the OTS and DLR implementation. Also, the integrated consideration of DLR and OTS within a unified framework offers a valuable avenue for future work to further enhance the flexibility region.

References

[1] C. Wang, Z. Gong, Y. Liang, W. Wei, and T. Bi, "Data-driven wind generation admissibility assessment of integrated electric-heat systems: A dynamic convex hull-based approach," *IEEE Transactions on Smart Grid,* vol. 11, no. 5, pp. 4531-4543, Sep. 2020, doi: https://doi.org/10.1109/TSG.2020.2993023.

[2] Z. Shen, W. Wei, T. Ding, Z. Li, and S. Mei, "Admissible region of renewable generation ensuring power flow solvability in distribution networks," *IEEE Systems Journal,* vol. 16, no. 3, pp. 3982-3992, Sept. 2022, doi: https://doi.org/10.1109/JSYST.2021.3138908.

[3] Y. Lei, B. Li, J. Meng, Y. Su, A. Li, and F. Liu, "The Changeable Region of Wind Power Considering Its Uncertainty," in 2020 12th IEEE PES Asia-Pacific Power and Energy Engineering Conference (APPEEC), Sep. 2020, pp. 1-5.

[4] J. Zhao, T. Zheng, and E. Litvinov, "Variable resource dispatch through do-not-exceed limit," IEEE *Transactions on Power Systems,* vol. 30, no. 2, pp. 820-828, Mar. 2014, doi: https://doi.org/10.1109/TPWRS.2014.2333367.

[5] C. Wang, F. Liu, J. Wang, W. Wei, and S. Mei, "Risk-based admissibility assessment of wind generation integrated into a bulk power system," *IEEE Transactions on Sustainable Energy,* vol. 7, no. 1, pp. 325-336, Nov. 2015, doi: https://doi.org/10.1109/TSTE.2015.2495299.

[6] Y. Zhang, X. Han, B. Xu, M. Wang, P. Ye, and Y. Pei, "Risk–based admissibility analysis of wind power integration into power system with energy storage system," *IEEE Access,* vol. 6, pp. 57400-57413, Sep. 2018, doi: https://doi.org/10.1109/ACCESS.2018.2870736.

[7] W. Wei, F. Liu, and S. Mei, "Dispatchable region of the variable wind generation," *IEEE transactions on power*

systems, vol. 30, no. 5, pp. 2755-2765, Sep. 2014, doi: https://doi.org/10.1109/TPWRS.2014.2365555.

[8] Y. Liu, Z. Li, Q. Wu, and H. Zhang, "Real-time dispatchable region of renewable generation constrained by reactive power and voltage profiles in AC power networks," *CSEE Journal of Power and Energy Systems,* vol. 6, no. 3, pp. 528-536, Sep. 2019, doi: https://doi.org/10.17775/CSEEJPES.2019.01620.

[9] Y. Liu, Z. Li, W. Wei, J. Zheng, and H. Zhang, "Data-driven dispatchable regions with potentially active boundaries for renewable power generation: concept and construction," *IEEE Transactions on Sustainable Energy,* vol. 13, no. 2, pp. 882-891, Apr. 2021, doi: https://doi.org/10.1109/TSTE.2021.3138125.

[10] H. Ji, C. Wang, P. Li, G. Song, H. Yu, and J. Wu, "Quantified analysis method for operational flexibility of active distribution networks with high penetration of distributed generators," *Applied Energy,* vol. 239, pp. 706-714, Apr. 2019, doi: https://doi.org/10.1016/j.apenergy.2019.02.008.

[11] J. Xiao, G. Zu, Y. Wang, X. Zhang, and X. Jiang, "Model and observation of dispatchable region for flexible distribution network," *Applied Energy,* vol. 261, pp. 114425, Mar. 2020, doi: https://doi.org/10.1016/j.apenergy.2019.114425.

[12] H. Huang, M. Zhou, S. Zhang, L. Zhang, G. Li, and Y. Sun, "Exploiting the operational flexibility of wind integrated hybrid AC/DC power systems," *IEEE Transactions on Power Systems,* vol. 36, no. 1, pp. 818-826, Jan. 2021, doi: https://doi.org/10.1109/TPWRS.2020.3014906.

[13] W. Dai, Z. Yang, J. Yu, K. Zhao, S. Wen, W. Lin, and W. Li, "Security region of renewable energy integration: Characterization and flexibility," *Energy,* vol. 187, pp. 115975, Nov. 2019, doi: https://doi.org/10.1016/j.energy.2019.115975.

[14] K. Wu, L. Wang, H. Ha, and Z. Wang, "Dynamic line rating and optimal transmission switching for maximizing renewable energy sources injection with voltage stability constraint," *Applied Energy,* vol. 378, pp. 124651, Jan. 2025, doi: https://doi.org/10.1016/j.apenergy.2024.124651.

[15] K. Wu, L. Wang, H. Ha, and M. Zhang, "Maximizing Wind Power Injection by Transmission Switching and DLR with Voltage Stability Constraints." Dec. 2024, pp. 659-664, doi: https://doi.org/10.1109/ICPSAsia61913.2024.10761389.

[16] E. B. Fisher, R. P. O'Neill, and M. C. Ferris, "Optimal transmission switching," *IEEE transactions on power systems,* vol. 23, no. 3, pp. 1346-1355, Aug. 2008, doi: https://doi.org/10.1109/TPWRS.2008.922256.

[17] M. Numan, M. F. Abbas, M. Yousif, S. S. Ghoneim, A. Mohammad, and A. Noorwali, "The role of optimal transmission switching in enhancing grid flexibility: A review," *IEEE Access,* vol. 11, pp. 32437-32463, Mar. 2023, doi: https://doi.org/10.1109/ACCESS.2023.3261459.

[18] E. Fernandez, I. Albizu, M. Bedialauneta, A. Mazon, and P. T. Leite, "Review of dynamic line rating systems for wind power integration," *Renewable and Sustainable Energy Reviews,* vol. 53, pp. 80-92, Jan. 2016, doi: https://doi.org/10.1016/j.rser.2015.07.149.

[19] "IEEE Standard for Calculating the Current-Temperature Relationship of Bare Overhead Conductors", IEEE Std 738-2023 (Revision of IEEE Std 738-2012), 1-56, 2023, doi: https://doi.org/10.1109/IEEESTD.2023.10382442.

[20] "Guide for thermal rating calculations of overhead lines", T. B. CIGRE, CIGRÉ, Paris, Dec. 2014, doi:

[21] D. Douglass, W. Chisholm, G. Davidson, I. Grant, K. Lindsey, M. Lancaster, D. Lawry, T. McCarthy, C. Nascimento, and M. Pasha, "Real-time overhead transmission-line monitoring for dynamic rating," *IEEE Transactions on Power Delivery,* vol. 31, no. 3, pp. 921-927, Jun. 2014, doi: https://doi.org/10.1109/TPWRD.2014.2383915.

[22] M. M. Esfahani, and G. R. Yousefi, "Real time congestion management in power systems considering quasi-dynamic thermal rating and congestion clearing time," *IEEE Transactions on Industrial Informatics,* vol. 12, no. 2, pp. 745-754, Apr. 2016, doi: https://doi.org/10.1109/TII.2016.2530402.

[23] J. Teh, and C.-M. Lai, "Reliability impacts of the dynamic thermal rating system on smart grids considering wireless communications," *IEEE Access,* vol. 7, pp. 41625-41635, Mar. 2019, doi: https://doi.org/10.1109/ACCESS.2019.2907980.

[24] M. Numan, D. Feng, F. Abbas, U. Rahman, and W. A. Wattoo, "Impact assessment of a co-optimized dynamic line rating and transmission switching topology on network expansion planning," *International Transactions on Electrical Energy Systems,* vol. 30, no. 8, pp. e12457, Jun. 2020, doi: https://doi.org/10.1002/2050-7038.12457.

[25] A. Bagheri, "Optimal transformer loss of life management in day-ahead scheduling of wind-rich power systems at the presence of dynamic ratings," *Electric Power Systems Research,* vol. 231, pp. 110259, Jun. 2024, doi: https://doi.org/10.1016/j.epsr.2024.110259.

[26] N. H. Abas, M. Z. A. Ab Kadir, N. Azis, J. Jasni, N. F. Ab Aziz, and Z. M. Khurshid, "Optimizing grid with dynamic line rating of conductors: A comprehensive review," *IEEE access,* vol. 12, pp. 9738-9756, Jan. 2024, doi: https://doi.org/10.1109/ACCESS.2024.3352595.

[27] W. Wei, F. Liu, and S. Mei, "Real-time dispatchability of bulk power systems with volatile renewable generations," *IEEE Transactions on Sustainable Energy,* vol. 6, no. 3, pp. 738-747, Jul. 2015, doi: https://doi.org/10.1109/TSTE.2015.2413903.

[28] K. W. Hedman, R. P. O'Neill, E. B. Fisher, and S. S. Oren, "Optimal transmission switching—sensitivity analysis and extensions," *IEEE Transactions on Power Systems,* vol. 23, no. 3, pp. 1469-1479, Aug. 2008, doi: https://doi.org/10.1109/TPWRS.2008.926411.

[29] J. D. Fuller, R. Ramasra, and A. Cha, "Fast heuristics for transmission-line switching," *IEEE Transactions on Power Systems,* vol. 27, no. 3, pp. 1377-1386, Aug. 2012, doi: https://doi.org/10.1109/TPWRS.2012.2186155.

[30] "Increasing Capacity of Overhead Transmission Lines–Needs and Solutions", T. B. CIGRE, CIGRÉ, Paris, 2010, doi:

[31] R. D. Zimmerman, C. E. Murillo-Sánchez, and R. J. Thomas, "MATPOWER: Steady-state operations, planning, and analysis tools for power systems research and education," *IEEE Transactions on power systems,* vol. 26, no. 1, pp. 12-19, Feb. 2010, doi: https://doi.org/10.1109/TPWRS.2010.2051168.

Appendix A

Determination of the Dominant two-Dimensional Subspace

This appendix formalizes the criterion for assigning a multi-dimensional ODP to its dominant two-dimensional subspace within the Radar Scanning algorithm framework. The dominant subspace for a given ODP is defined as the plane spanned by the two coordinate axes corresponding to its components with the largest absolute magnitudes.

Formal Description: Let an ODP be represented by an n-dimensional vector W= ($\omega_1, \omega_2, \ldots, \omega_n$). The algorithm identifies the indices {i, j} of the two components with the largest magnitude values, such that $|\omega_i| \geq |\omega_j| \geq |\omega_k|$ for all $k \notin \{i, j\}$. The dominant subspace for this ODP is then defined by the orthogonal axes ω_i and ω_j. The ODP is subsequently projected onto this (ω_i, ω_j) plane for all subsequent analysis and clustering operations within the Radar Scanning method.

Illustrative Example: Consider a system analyzed in a 3-dimensional parameter space with axes ($\omega_1, \omega_2, \omega_3$). For an ODP W= (2.5, 2.7, 2.2), the magnitude values are $|\omega_1| = 2.5$, $|\omega_2| = 2.7$ and $|\omega_3| = 2.2$. The ranking of magnitudes yields $|\omega_2| > |\omega_1| > |\omega_3|$. Consequently, the dominant subspace for this point is defined by the axes ω_2 and ω_1. All geometric and clustering calculations for this ODP within the Radar Scanning algorithm are performed within this (ω_1, ω_2) plane. This deterministic assignment is performed for every ODP in the dataset. The collective result is an efficient partition of the high-dimensional data across relevant 2D subspaces, which is fundamental to the computational efficiency of the proposed algorithm. A complete numerical demonstration for a sample dataset is provided in Table A-1.

Table A-1: Example of Determining the Dominant 2D Subspace for ODPs.

ODP	First output amplitude value (ω_1 axis)	Second output amplitude value (ω_2 axis)	thirst output amplitude value (ω_3 axis)	the dominant 2-dimensional space
1	2.2	2.7	2.5	(, $\omega_3\omega_2$)
2	5	9	10	(ω_2, ω_3)
3	-5	0	3	(ω_1, ω_3)
4	4	8	9	(ω_2, ω_3)
5	4	4	2	(, $\omega_2\omega_1$)

Once each ODP is assigned to its dominant 2D subspace (e.g., as detailed in Table A-1), the algorithm performs all data clustering and flexibility region determination within these subspaces. This approach reduces the problem's dimensionality, leading to a significant decrease in computational load and processing time while maintaining the solution precision.

Ali Beiranvand received the B.S. and M.S. degrees in electrical engineering from Shahid Chamran University of Ahvaz, Ahvaz, Iran, in 2009 and 2012, respectively. He is currently pursuing the Ph.D. degree in Power engineering at Lorestan University, KhoramAbad, Iran. His research interests include power system optimization, integration of renewable energy resources, Dynamic Line Rating systems and design of overhead transmission lines.

MahmoodReza Shakarami was born in KhorramAbad, Iran in 1972. He received his M.Sc. and Ph.D. degree in Electrical Engineering from the Iran University of Science and Technology, Tehran, Iran, in 2000 and 2010, respectively. He is currently an Associate Professor in Electrical Engineering Department of Lorestan University, KhorramAbad, Iran. His current research interests include power system dynamics and stability, FACTS devices, and distribution systems.

Meysam Doostizadeh received the MSc and Ph.D. degrees in Electrical Engineering from the University of Tehran, Tehran, Iran, in 2012 and 2016, respectively. He is currently an Associate Professor with the Faculty of Engineering, Lorestan University, KhorramAbad, Iran. His research interests include power system optimization, electricity markets, smart grid technologies, and integration of renewable energy into power systems.